Available online at www.sciencedirect.com
ScienceDirect
Polymer 47 (2006) 8326–8336
polymer
www.elsevier.com/locate/polymer

Water transport in densely crosslinked networks: A comparison between epoxy systems having different interactive characters

G. Mensitieri [a], M. Lavorgna [b], P. Musto [c,*], G. Ragosta [c]

[a] Department of Materials and Production Engineering, University of Naples Federico II, P.le Tecchio 80, 80125 Naples, Italy
[b] Institute of Composite and Biomedical Materials, National Research Council of Italy, P.le Tecchio 80, 80125 Naples, Italy
[c] Institute of Chemistry and Technology of Polymers, National Research Council of Italy, Via Campi Flegrei, 34, 80078 Pozzuoli, Naples, Italy

Received 16 June 2006; received in revised form 15 September 2006; accepted 17 September 2006
Available online 30 October 2006

Abstract

Water transport in a densely crosslinked epoxy network, TGDDM–HHPA, was investigated by coupling time-resolved FTIR spectroscopy and gravimetric measurements. Vibrational analysis yielded information on the different water species present in the system and allowed a quantitative estimation of their population at sorption equilibrium.

The transport of water molecules was found to follow a Fickian behaviour characterized by an effective diffusion coefficient which increases with total water concentration. The dependence of the effective diffusion coefficient, $D_{\text{eff}}(C)$, on concentration, as obtained from integral sorption curves, was interpreted by introducing a concentration dependent term, $D(C)$, and an ''interaction factor'', ϕ, which accounts for the effect of the molecular interactions which effectively slow down the diffusion process.

The results were compared with those obtained on another epoxy network, TGDDM–DDS, characterized by the presence of stronger interacting sites. Differences and similarities of the spectroscopic and gravimetric results are critically discussed in the light of the structure of the two networks.

Keywords: Diffusion; Epoxy resins; FTIR spectroscopy

1. Introduction

Although the epoxy resins were first synthesized in the early 1940s, they still represent one of the most actively investigated classes of thermosetting materials [1–3]. This is due to their good mechanical and thermal properties, high resistance to solvents and corrosive agents, excellent adhesion to various substrates, low shrinkage upon curing and easy processing under a wide range of conditions. The above characteristics make epoxy resins very attractive in several demanding areas as, for example, the encapsulation of microcircuitry in the electronic industry, the development of specialized coatings for highly aggressive environments, and in aerospace applications [1–4].

In particular, the tetrafunctional monomer tetraglycidyl-4,4′-diaminodiphenylmethane (TGDDM) produces networks with very high crosslink density, which is reflected in T_g values exceeding 270 °C, and outstanding physico-mechanical properties: for this reason TGDDM cured with aromatic diamine hardeners such as 4,4′-diamino diphenylsulphone (DDS) are the preferred resin systems for use as matrices in high performance fiber composites for aerospace applications. One major deficiency of these formulations is the absorption of relatively large amounts of water in high humidity environments (up to 7% by weight), which brings about a general deterioration of properties [5–8]. The use of an anhydride hardener such as hexahydrophtalic anhydride (HHPA) may result in a number of distinct advantages in comparison to DDS. Of utmost importance are the reduced toxicity of the hardener and the decrease in water sorption it imparts to the formulations. Other relevant advantages are a smaller shrinkage, and

* Corresponding author. Tel.: +39 081 8675202; fax: +39 081 8675230.
E-mail address: musto@ictp.cnr.it (P. Musto).

0032-3861/$ - see front matter © 2006 Elsevier Ltd. All rights reserved.
doi:10.1016/j.polymer.2006.09.066

a lower reaction exothermicity [1–3]. The difference in water sorption between the two TGDDM based formulations has been generally ascribed to a lower tendency of the HHPA based resins to interact with penetrant molecules. No systematic investigations have been performed, however, to address this issue on a quantitative basis, possibly because of the lack of suitable experimental approaches.

In recent years, a number of investigators recognized the potential of applying FTIR spectroscopy to diffusion studies [9–14]. This technique provides several important advantages, i.e. the high sampling rate, the sensitivity and accuracy of the quantitative analysis and, above all, the wealth of information at molecular level contained in the vibrational spectrum [9–12].

In the present contribution the sorption and desorption of water in a thin film of TGDDM–HHPA are investigated by means of in situ, *time-resolved* FTIR spectroscopic measurements in the transmission mode. This technique provides not only a means for monitoring accurately the penetrant sorption kinetics but offers also the possibility of studying in detail the concurrent development of molecular interactions, thus identifying the type of molecular aggregates and the sites involved in the interactions.

With respect to the penetrant molecule, the attention has been focused onto the fundamental O–H stretching vibrations, these being the most sensitive to H-bonding; the H–O–H bending region has been analysed as well. For the polymer network, the perturbation of the carbonyl region and of the characteristic aromatic peaks as a function of the total water content has been investigated. Sorption tests have been performed also by gravimetric analysis at several water vapour activities to gather a deeper understanding of the absorbance–mass relationship. A close correspondence was obtained between the gravimetric determination of the total water content and the spectroscopic estimation based on the knowledge of the molar absorptivities of the various water species present in the system.

The results obtained in the present contribution were eventually compared with those gathered on a TGDDM–DDS epoxy network, characterized by the presence of stronger interacting sites. The different behaviour of the two formulations with respect to mass transport and the tendency to interact at molecular level with water were critically discussed in the light of the structure of the two networks.

2. Materials and methods

2.1. Materials

The epoxy resin was a commercial grade tetraglycidyl-4,4′-diaminodiphenylmethane (TGDDM) supplied by Ciba Geigy (Basel, Switzerland), and the curing agent was hexahydrophtalic anhydride (HHPA) from Sigma–Aldrich, Italy (Milan, Italy). HHPA (69 g) was dissolved in 100 g of TGDDM at room temperature, degassed under vacuum, and poured between two stainless steel plates. A pressure of 100 bar was applied in a compression moulding press to obtain thin films [thickness $(L) = 22 \pm 0.5$ μm]. The first step of the curing schedule was conducted at 140 °C for 16 h, followed by a post-curing step at 200 °C for 5 h. The T_g of the material, taken as the tan δ peak in the dynamical–mechanical spectrum, was 160 °C. The density of the fully cured network was 1.225 g/cm^3, as determined by helium picnometry. The preparation procedure and the curing schedule for the TGDDM–DDS resin are detailed in Ref. [8].

2.2. Techniques

2.2.1. Water sorption by in situ, time-resolved FTIR spectroscopy

A vacuum tight FTIR cell was designed and constructed to monitor the FTIR transmission spectra of the polymer films exposed to a controlled humidity environment. The cell is connected through service lines to a water reservoir and to vacuum and pressure transducers. The details of the experimental apparatus are reported elsewhere [12,15].

The FTIR spectrometer was a Perkin–Elmer System 2000 equipped with a Germanium/KBr beam splitter and a wide-band DTGS detector. Instrumental parameters for *time-resolved* data collection were as follows: resolution = 4 cm^{-1}, optical path difference (OPD) velocity = 0.2 cm s^{-1}, spectral range 4000–400 cm^{-1}. A single data collection was performed for each spectrum which, under the selected instrumental conditions, took 6 s to complete. The signal was acquired as a single beam spectrum at specific time intervals which increased as the sorption process approached equilibrium. A typical sorption run lasted for about 90 min and acquisition time intervals were 6 s during the first 10 min of the experiment and 60 s afterwards. The spectra at sorption equilibrium to be used for the curve resolving analysis were collected under different instrumental conditions, i.e. at a resolution of 0.5 cm^{-1} and by signal-averaging of 256 consecutive scans. This is in order to maximize the number of data points in the frequency region of interest and for improving the signal-to-noise ratio.

Sorption–desorption tests were performed at 24 °C and at relative pressures, p/p_0, of 0.08, 0.2, 0.4 and 0.6 (where p is the experimental pressure and p_0 is the saturation pressure of water vapour at 24 °C, corresponding to 22.38 Torr). Assuming ideal behaviour for the water vapour phase, the relative pressure can be assumed to be coincident with the water vapour activity, a_w.

Before each sorption test, the sample was dried in the FTIR cell kept under vacuum (1.0×10^{-3} Torr) at 24 °C, until complete disappearance of the characteristic water bands. Afterwards, the cell was brought at the desired pressure level and the data acquisition was started. Once an apparent sorption equilibrium was attained, the cell was evacuated again and the desorption process was monitored.

2.2.2. Gravimetric analysis

The equipment used to determine the weight gain of the samples exposed to a controlled humidity environment was essentially the same as that used for the on-line FTIR spectroscopic measurements, with the FTIR measuring cell being

replaced by an electronic microbalance, model D200 (CAHN Instruments, Madison, WI), with a sensitivity of 0.1 μg.

Water sorption kinetics are reported as normalized sorbed mass versus time. Normalized sorbed mass is defined as the ratio between the mass at time t, M_t, and the corresponding value at sorption equilibrium, M_∞.

2.2.3. Data analysis

For the sorption tests, the absorbance spectra were obtained by ratioing the single beam spectra against a background collected on the cell with no sample inside, kept at the same water vapour pressure as the sorption test to be performed. Examples of absorbance spectra collected at the beginning of a sorption test (*dry* sample) and after equilibration with water vapour at $a_w = 0.4$ (*wet* sample) are reported in Fig. 1. For the desorption tests the background was collected on the empty cell evacuated to 1.0×10^{-3} Torr. The spectra of sorbed water at different times were isolated by eliminating the interference of the polymer matrix in the regions of interest. To this end subtraction spectroscopy was used [16,17], i.e.:

$$A_d = A_s - KA_r \quad (1)$$

where A is the absorbance, the subscripts d, s and r denote, respectively, the difference spectrum, the sample spectrum (*wet* sample) and the reference spectrum (*dry* sample) and K is the subtraction factor, i.e. an adjustable parameter which accounts for possible thickness changes between the sample and reference spectra [8,16,17]. In our case, since the sample thickness remains essentially constant upon water sorption, K was consistently taken as equal to unity.

In order to separate the individual peaks in the case of unresolved, multicomponent bands, a curve resolving algorithm was employed, based on the Levenberg–Marquardt method [18,19]. In order to reduce the number of adjustable parameters and to insure the uniqueness of the result, the baseline, the band shape and the number of components were fixed. The Voigt model was consistently employed to simulate the experimental profiles of the band components [20]. Sorption kinetic data evaluated by FTIR spectroscopy are reported as the absorbance ratio of the ν_{OH} or δ_{HOH} water band versus the square root of time. The absorbance ratio is defined as the ratio between the absorbance at time t (A_t), and the corresponding value at sorption equilibrium (A_∞).

3. Results and discussion

3.1. Molecular interactions and equilibrium sorption

The spectrum of the TGDDM–HHPA resin after equilibration with water vapour at $a_w = 0.4$ (Fig. 1) displays features characteristic of sorbed water at around 3530, 1630, and 550 cm^{-1}. These arise, respectively, from the stretching vibrations (ν_{OH}), the bending modes (δ_{HOH}) and the vibration modes (i.e. hindered rotations) of the H_2O molecule.

Elimination of the interference from the matrix spectrum, by means of subtraction analysis (see experimental) allows us to isolate the spectrum of sorbed water in the regions of interest. The bands relative to the stretching and bending modes are reported, respectively, in Figs. 2 and 3. Fig. 2 also displays the results of the curve-fitting analysis which will be discussed in detail later.

The ν_{OH} band shows a sharp peak at 3636 cm^{-1} superimposed onto a broader profile at lower wavenumbers. Following the vibrational analysis reported in Refs. [8,12,15], we assign the 3636 cm^{-1} component to water molecules whose hydrogen atoms are not involved in H-bonding interactions (referred to as S_0 species, according to the nomenclature in Ref. [8]). Conversely, the broad profile at lower frequencies is indicative of H-bonded species and the fine structure evident in the band shape is suggestive of a multiplicity of molecular aggregates. These molecular interactions are reflected also in the shape of the bending absorption, albeit with less details due to lower sensitivity of this vibrational mode to H-bonding interactions. In Fig. 3 only two rather symmetrical components are evident, centred, respectively, at 1628 and 1614 cm^{-1}. The sharper component at lower frequency is assigned to non-interacting

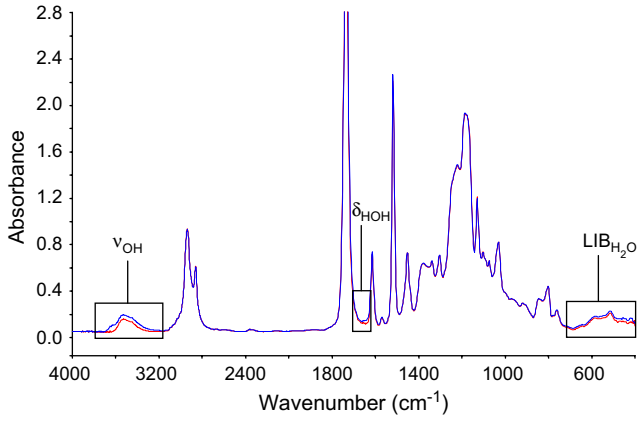

Fig. 1. FTIR spectra in the 4000–400 cm^{-1} range for the TGDDM–HHPA resin in the dry state (red trace) and after equilibration at $a_w = 0.4$ (blue trace). Sample thickness = 22 ± 0.5 μm. (For interpretation of the references to color in this figure legend, the reader is referred to the web version of this article.)

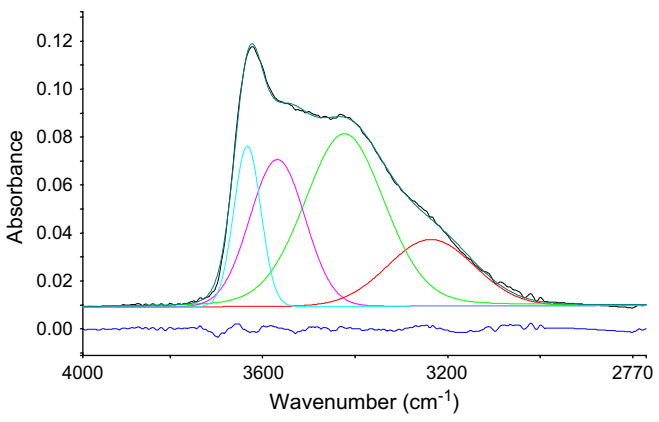

Fig. 2. Subtraction spectrum after equilibration with water vapour at $a_w = 0.4$ in the ν_{OH} region (3900–2800 cm^{-1}). The figure also displays the curve-fitting analysis of the subtraction spectrum, i.e. the four resolved components, the simulated curve, and the residual (i.e. experimental spectrum–simulated spectrum).

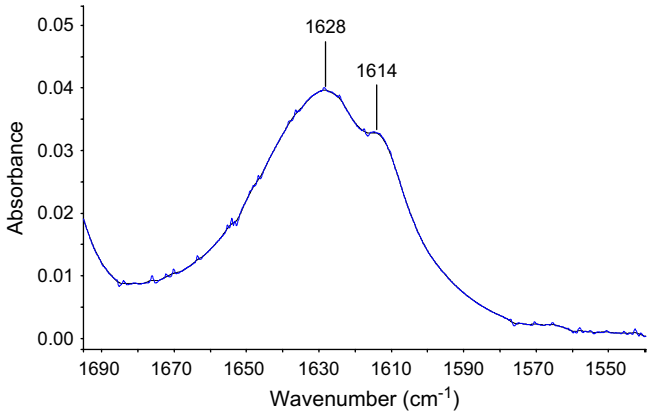

Fig. 3. Subtraction spectrum after equilibration with water vapour at $a_w = 0.4$ in the δ_{HOH} region (1690–1550 cm^{-1}). The figure displays the experimental profile (blue trace) and the smoothed profile (Savitzky–Golay method, 9 points, black trace). The spectrum has been collected at a resolution of 0.5 cm^{-1}.

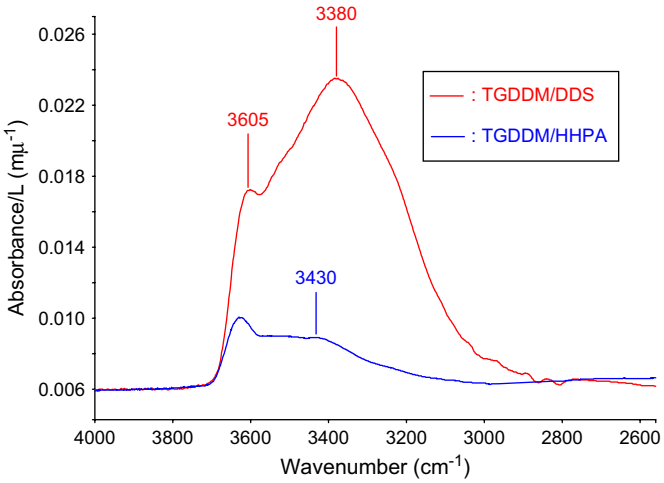

Fig. 4. Subtraction spectra normalized for film thickness, in the ν_{OH} region (4000–2560 cm^{-1}). Samples (TGDDM–DDS, red trace and TGDDM–HHPA, blue trace) equilibrated at a water vapour activity, a_w, of 0.4.

H_2O molecules, while the broader band shifted at higher frequency is attributed to the multiplicity of interacting water species. This is because the formation of an H-bonding interaction, due to its highly directional character, causes a stiffening of the force constant relative to the in-plane deformation, which is reflected in a blue-shift proportional to the interaction strength [21,22]. The effect is exactly opposite to that observed in the stretching region, whereby the interaction causes a weakening of the force constant and a consequent red-shift. A different behaviour is also reported in the two frequency regions in terms of the enhancement of the integrated intensity of the respective vibrational modes [21–23]. In fact, a conspicuous increase (up to an order of magnitude) of molar absorptivity is found for the stretching modes as a consequence of the directionality of the H-bonding, which enhances the derivative of the transition moment with respect to the relative normal coordinate. A much lower effect is observed for the bending modes, which are reported to undergo a twofold absorptivity enhancement, at the most [21–23]. We wish to emphasize the occurrence, both in the ν_{OH} and in the δ_{HOH} regions, of partially resolved components whose shape is much sharper than that of the rest of the respective profiles and whose frequency is considerably shifted with respect to the main absorption and is consistent with the frequency expected for a non-interacting H_2O molecules. In our opinion this is to be taken as a firm experimental evidence for the presence of water molecules not involved in H-bonding as proton donors (which we refer to as "free" water or S_0 species) in TGDDM based epoxy resins.

On the basis of the experimental observation that anhydride cured epoxies absorb less water than their amine-cured counterparts, it has been postulated that the former systems are less interactive towards water [1–3]. The present spectroscopic analysis provides the possibility to confirm this hypothesis and to quantify the effect. In fact, a direct comparison between the spectra (normalized for sample thickness) of water sorbed in TGDDM–HHPA (Fig. 4, blue trace) and in TGDDM–DDS (Fig. 4, red trace) clearly indicates that the amine-cured system not only displays a larger amount of sorbed water, but also that, in the latter system, the population of interacting water molecules increases substantially. Moreover, the 50 cm^{-1} red-shift of the low-frequency band characteristic of the interacting species points to the establishment, in the TGDDM–DDS system, of stronger H-bonding interactions. This is not surprising, in view of the presence, within the TGDDM–DDS network, of strong proton acceptor groups (i.e. amino-alcohol, sulphone) which are replaced by weaker proton acceptors (i.e. ester carbonyls) in the case of TGDDM–HHPA [21,22].

The analysis of the difference spectra in the 2000–500 cm^{-1} region provides further evidence for the unambiguous identification of the interacting sites onto the TGDDM–HHPA network. This analysis has been performed on a thinner sample (14.0 ± 0.5 μm) in order to keep the intense carbonyl band in the range of absorbance–concentration linearity (i.e. within 1.6 absorbance units).

In Fig. 5, traces B–E, are reported the difference spectra obtained by subtracting the spectrum of the dry resin (trace A) from the spectra of the samples equilibrated at various water vapour activities. A number of features are observed which become increasingly pronounced as the water activity raises. First-derivative type bands, displaying a minimum and a maximum at close wavenumbers, are indicative of peak shifts, i.e. a frequency displacement of the peak in the sample spectrum (*wet resin*) with respect to the peak position in the reference spectrum (*dry resin*). In particular, when the negative lobe precedes the positive (i.e. occurs at higher wavenumbers), displacement takes place towards lower frequencies. A prominent first-derivative profile is observed at 1760 cm^{-1} (minimum) and 1710 cm^{-1} (maximum). It is associated with the carbonyl peak centred at 1733 cm^{-1} in the dry resin and demonstrates the involvement of this group as proton acceptor in H-bond formation with water molecules. The positive band at 1632 cm^{-1} is the bending mode of absorbed water. At lower wavenumbers two fully resolved peaks are observed at 1515 and 1451 cm^{-1}. These features are barely detectable compared to the other effects observed in the difference spectra, but are reproducible and fully reversible (see later discussion). The

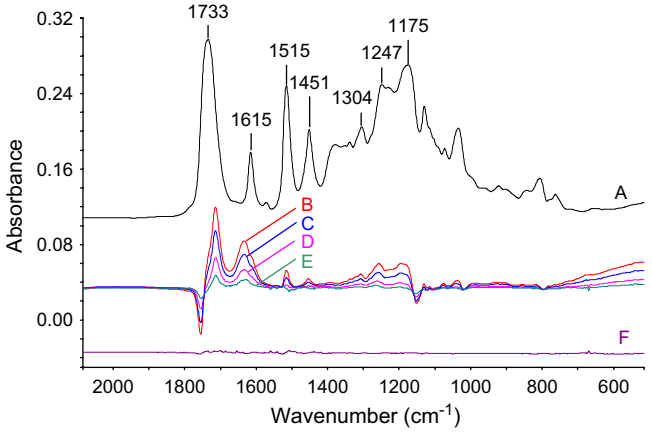

Fig. 5. Trace A: FTIR spectrum in the 2000–600 cm^{-1} range for the TGDDM–HHPA resin in the dry state. Trace B: spectrum of the sample equilibrated at $a_w = 0.6$ minus the spectrum of the dry sample. Trace C: spectrum of the sample equilibrated at $a_w = 0.4$ minus the spectrum of the dry sample. Trace D: spectrum of the sample equilibrated at $a_w = 0.2$ minus the spectrum of the dry sample. Trace E: spectrum of the sample equilibrated at $a_w = 0.08$ minus the spectrum of the dry sample. Trace F: spectrum of the sample equilibrated at $a_w = 0.6$ and fully desorbed minus the spectrum of the dry sample.

two peaks are related to the aromatic bands of the TGDDM unit and reflect their slight intensity increase as a consequence of the interaction with absorbed water. A thickness effect, i.e. an increase of the path length related to sample swelling, can be ruled out since it would produce an intensity decrease. This spectroscopic evidence could be tentatively ascribed to an interaction between the protons of water molecules and the π-electron cloud of the di-substituted aromatic rings [24–26]. Contrary to what happens for stronger H-bonding interactions, which produce a shift in the peak positions of the groups involved, in this case only an intensity effect is detected. This indicates that the interaction slightly alters the transition moment vector of the normal mode (i.e. it affects the polarity) but is unable to produce a detectable alteration of the force constants involved in the vibration. Rather complex features are observed below 1400 cm^{-1}, likely related to the complex, conformationally sensitive ν_{C-O-C} multiplet. Although the difference spectrum in this region is not 'clean', the above effect could be ascribed either to the involvement of the C–O–C group in H-bonding interactions with water molecules or to a perturbation of the conformational equilibrium (i.e. a change in the relative population of rotamers) around the C–O–C bonds.

It is worth noting that all the effects discussed so far are fully reversible upon complete desorption of water, as demonstrated in Fig. 5, trace F, which represents the subtraction between the spectrum of a sample equilibrated at $a_w = 0.6$ and subsequently desorbed, and the spectrum of the initial dry sample. This further confirms that the features observed in the subtraction spectra originate from molecular interactions between the penetrant and the substrate and not from chemical reactions (e.g. hydrolysis) or spectroscopic artefacts.

Towards a quantitative assessment of the population of the different water species present in the system, we applied a method already discussed in Ref. [8] based on the curve fitting of the ν_{OH} region (4000–2770 cm^{-1}, see Fig. 2). This method relies on the relationship between the shift of the ν_{O-H} peak ($\Delta\nu$) and the absorptivity change, $\Delta\varepsilon$, according to Huggins and Pimentel [27] and Mirone and Fabbri [28]. The above $\Delta\nu - \Delta\varepsilon$ relationship, together with the value of the molar absorptivity of unassociated water (ε_{S_0}) taken from Ref. [8], affords an estimation of the absorptivity values of the different water species.

The results of these calculations are summarized in Table 1, column 5. It is noted that the absorptivity ratio between associated and free species is equal to 2.8, 5.8 and 8.1, respectively, for the species absorbing at 3565, 3436 and 3270 cm^{-1}. The above ratios are consistent with those expected for systems forming medium-to-high H-bonding interactions, for which absorptivity enhancements up to an order of magnitude have been reported [21,22].

Table 1
Curve-fitting results, molar absorptivities and concentration of water species as evaluated spectroscopically and gravimetrically

Activity	Position (cm^{-1})	FWHH (cm^{-1})	Area (cm^{-1})	$\varepsilon_i \times 10^{-6}$ (cm/mol)	C_i (wt%)	$C_{TOT\ FTIR}$ (wt%)	$C_{TOT\ GRAV}$ (wt%)	C_{FTIR}/C_{GRAV}
0.08	3630	68	1.63	8.66	0.12	0.27	0.25	1.08
	3565	140	2.63	24.67	0.07			
	3417	201	5.12	50.11	0.06			
	3239	229	2.11	70.33	0.019			
0.2	3632	68	3.00	8.66	0.226	0.51	0.48	1.06
	3568	140	5.23	24.67	0.138			
	3420	205	9.50	50.11	0.12			
	3237	218	3.57	70.33	0.03			
0.4	3633	69	4.90	8.66	0.369	0.87	0.86	1.02
	3568	140	9.13	24.67	0.241			
	3423	204	15.97	50.11	0.207			
	3236	220	6.48	70.33	0.058			
0.6	3632	71	6.58	8.66	0.496	1.19	1.28	0.93
	3567	140	12.19	24.67	0.323			
	3425	201	21.9	50.11	0.285			
	3237	224	9.00	70.33	0.081			

The knowledge of the absorptivities of the various water species allows us to transform the absorbance values into concentration according to:

$$C_{TOT} = C_{S_0} + \sum_{i=1}^{n} C_i = C_{3632} + C_{3565} + C_{3436} + C_{3270} = \frac{1}{L}\left(\frac{A_{3632}}{\varepsilon_{3632}} + \frac{A_{3565}}{\varepsilon_{3565}} + \frac{A_{3436}}{\varepsilon_{3436}} + \frac{A_{3270}}{\varepsilon_{3270}}\right) \quad (2)$$

Here C_{TOT} is the total concentration of sorbed water, n is the total number of different types of H-bonded water species and L is the sample thickness.

On the basis of the procedure outlined above, a fully spectroscopic estimate (i.e. with no calibration against an absolute technique) of the total concentration of absorbed water (Table 1, column 7) and of the concentration of each species (Table 1, column 6) can be obtained. The values of the total concentration of water absorbed at equilibrium at the four investigated activities, as evaluated gravimetrically and by FTIR spectroscopy, are compared in Table 1, columns 7–9. As already observed for the case of the TGDDM–DDS system [8], an excellent agreement between the spectroscopic and the gravimetric determinations is obtained at all investigated activities, which adds to the reliability of the assumptions upon which the FTIR analysis is based.

The plot of the relative concentration of non-interacting water species as a function of water vapour activity (Fig. 6) demonstrates, in a quantitative fashion, the lower interacting character of the TGDDM–HHPA resin with respect to the TGDDM–DDS. In fact, for both systems the ratio C_{S_0}/C_{TOT} is roughly constant in the investigated activity range, and is larger by a factor of 1.25 for the TGDDM–HHPA resin. The increased interactive character of the DDS containing network is also reflected in a higher amount of water sorbed at equilibrium, as is evident from the sorption isotherms reported in Fig. 7. This result is relevant for technological applications, in view of the well known worsening of end-properties caused by the plasticizing effect of sorbed water.

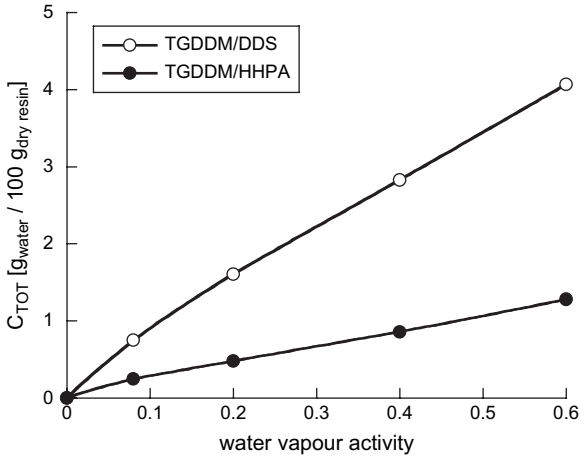

Fig. 7. Sorption isotherms in the 0–0.6 activity range for the TGDDM–HHPA resin (●) and the TGDDM–DDS resin (○).

In Fig. 8 are reported the equilibrium concentrations of the different water species as a function of total water concentration as measured spectroscopically for TGDDM–HHPA. A linear dependence is evident for all the species, which points to a linear equilibrium among them. An analogous behaviour has been observed for the case of the TGDDM–DDS/water system [8].

3.2. Dynamics of mass transport

Water sorption kinetics for TGDDM–HHPA at different activities have been determined both spectroscopically and gravimetrically. In particular, from the FTIR data, two independent estimations of the water content can be achieved using, respectively, the OH stretching band and the H–O–H bending signal of sorbed water. Sorption kinetics at $a_w = 0.4$ obtained from on-line FTIR experiments and from gravimetric

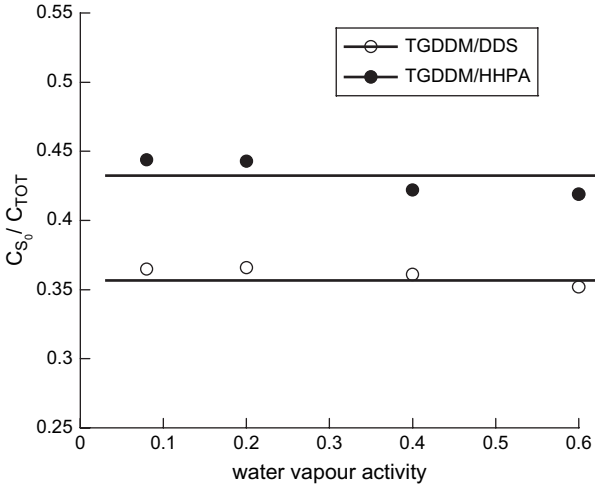

Fig. 6. Relative concentration of non-interacting water as a function of water vapour activity for the TGDDM–HHPA resin (●) and the TGDDM–DDS resin (○).

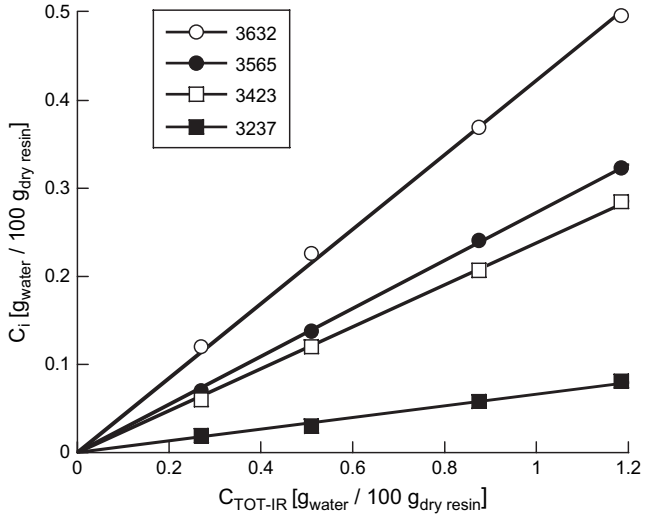

Fig. 8. Concentration of the different water species as a function of the total amount of sorbed water for the TGDDM–HHPA resin.

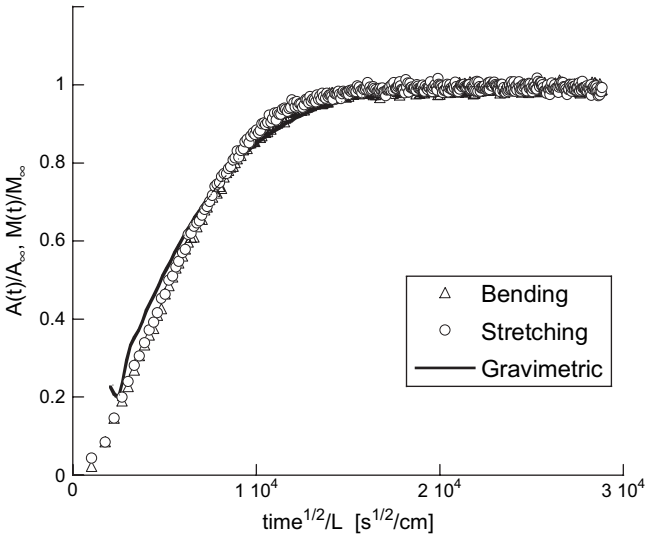

Fig. 9. Sorption kinetics at $a_w = 0.4$ for the TGDDM–HHPA resin. (△) Spectroscopic measurement using the δ_{HOH} band; (□) spectroscopic measurement using the ν_{OH} band; (○) gravimetric measurement.

measurements are compared in Fig. 9. The curves relative to the bending and the stretching signals are coincident, and a reasonably good superposition is also observed with the gravimetric data. The coincidence of bending and stretching curves has been found at all the investigated activities. This is demonstrated in Fig. 10 where the spectroscopic data are reported in the form of an absorbance–absorbance diagram. As predicted by the Beer–Lambert relationship, all data points can be accommodated on a single master line, passing through the origin.

In interpreting these results, it is to be considered that, while the molar absorptivities of the various components are significantly different in the ν_{OH} water band (see Table 1), the absorptivities in the bending region are nearly constant [27,28]. Therefore, if the concentration ratio among the water species changed with time during the dynamic sorption test, this would produce a significant non-linearity in an absorbance–absorbance plot. Therefore, the observed linear behaviour points to the establishment of a local equilibrium among the various water species, which is 'instantaneous' as compared to the characteristic time of diffusion, which is of the order of 10^3 s. This equilibrium is coincident with that attained at the end of the sorption process.

In Fig. 11 are compared sorption–desorption cycles, as determined spectroscopically (ν_{OH} band) for TGDDM–DDS and TGDDM–HHPA samples exposed to water vapour at $a_w = 0.4$. For both samples, sorption is faster than desorption, indicating that water diffusivity is an increasing function of concentration [29]. The sorption–desorption lag is more pronounced for the TGDDM–DDS resin, indicating a stronger dependence of sorption kinetics on water concentration than for TGDDM–HHPA. This concentration dependence is also evident when considering the sorption experiments performed at different activities (see Fig. 12A and B). In fact it is observed that, for both resins, the sorption rate, and consequently the effective diffusivity, increases with water activity. Again, this effect is more pronounced in the case of the TGDDM–DDS system.

In interpreting the sorption kinetic results, it should be considered that the molecular mechanisms involved in the transport are: (1) diffusion of water molecules through the polymer matrix, which is concentration dependent due to the free volume increase associated with solubilization; (2) interactions of water molecules with specific sites distributed on the polymer network, that slow down the diffusion process.

As discussed in a previous paper on TGDDM–DDS [8], this latter effect could be accounted for by a model which assumes that diffusion is associated with the reversible formation of molecular aggregates between water molecules and interaction sites. In view of the experimental results, which

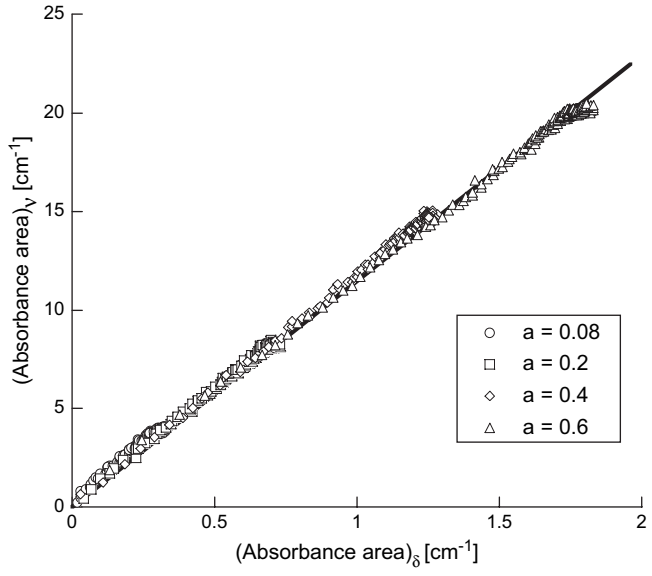

Fig. 10. Absorbance area of the ν_{OH} band versus the absorbance area of the δ_{HOH} band for sorption kinetics at different water vapour activities.

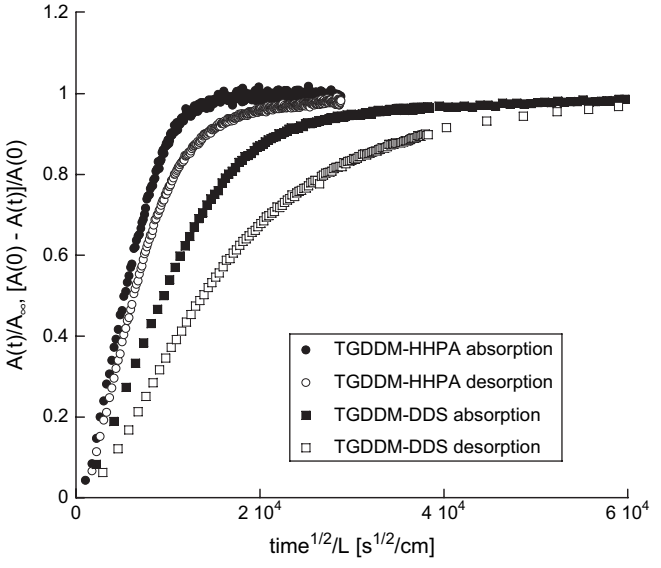

Fig. 11. Sorption–desorption cycles at $a_w = 0.4$ as evaluated spectroscopically from the absorbance area of the ν_{OH} band for the TGDDM–HHPA resin and for the TGDDM–DDS resin.

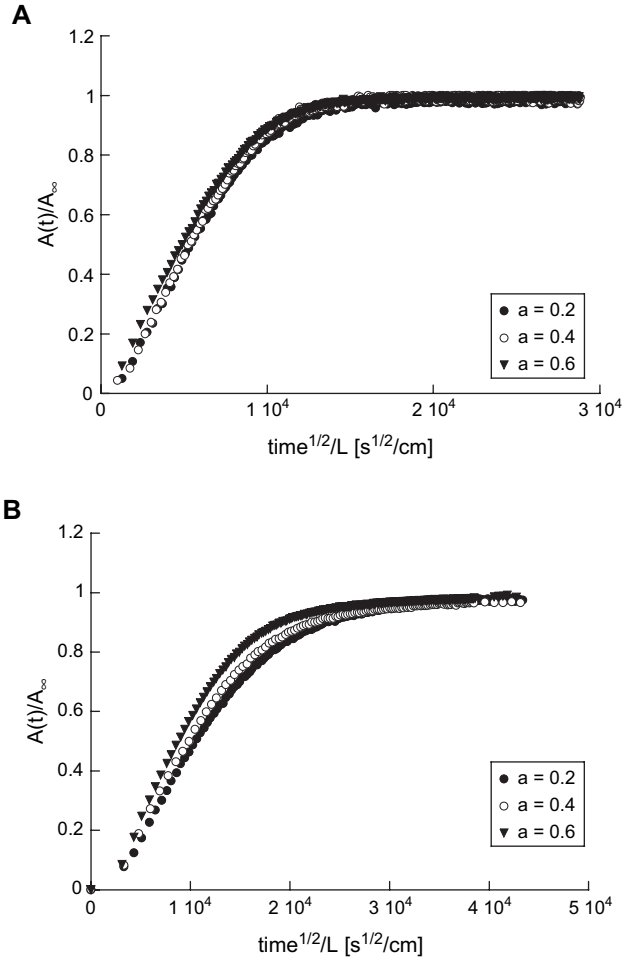

Fig. 12. (A) Sorption kinetics at different activities for the TGDDM–HHPA resin, as evaluated spectroscopically from the absorbance area of the ν_{OH} band. (B) Sorption kinetics at different activities for the TGDDM–DDS resin, as evaluated spectroscopically from the absorbance area of the ν_{OH} band.

point, for both TGDDM–DDS and TGDDM–HHPA, to the establishment of an *instantaneous local equilibrium* among the various water species, it has been further assumed that a 'Langmuir-type' absorption equilibrium relates the concentration of 'free' water molecules (C_{S_0}) to the concentration of 'bound' water molecules (C_i):

$$C_i = \frac{K_i C_{S_0} C_i^0}{1 + K_i C_{S_0}} \tag{3}$$

where K_i's are taken as constants and C_i^0 is the concentration of sites of type i available on the backbone. It is worth noting that we use here the term 'Langmuir-type' absorption in the sense that, with regard to bound and free water molecules, the equilibrium is similar to that described by the Langmuir theory for adsorption isotherms, although here we are dealing with a bulk absorption, with no involvement of free surfaces (for a discussion on this point see Ref. [30]).

Furthermore, the model is based on the presumption that water molecules involved in these interactions have a negligible mobility as compared to 'free' water molecules. As a consequence the differential mass balance for 'free' water species reads [8]:

$$\phi^{-1}\frac{\partial C_{S_0}}{\partial t} = \frac{\partial}{\partial x}\left(D(C_{TOT})\frac{\partial C_{S_0}}{\partial x}\right) \tag{4}$$

where:

$$\phi^{-1} = 1 + \sum_{i=1}^{n}\frac{C_i^0 K_i}{(1 + K_i C_{S_0})^2} \tag{5}$$

Whenever the *instantaneous local equilibrium* established among the various water species is *linear*, as it is experimentally observed in both the TGDDM–DDS and TGDDM–HHPA systems, the 'interaction factor', ϕ, assumes a particularly simple form, which is independent of water concentration:

$$\phi = \left(1 + \sum_{i=1}^{n} K_i C_i^0\right)^{-1} = \left(1 + \sum_{i=1}^{n}\frac{C_i}{C_{S_0}}\right)^{-1} \tag{6}$$

In these circumstances, the value of ϕ can be easily evaluated from the spectroscopic data reported in Table 1. Since the adopted Langmuir-type absorption model is non-linear, the experimentally observed establishment of a linear equilibrium among the different water species should be concurrently accompanied by the further condition that the interacting sites (ester carbonyls, among others, in the case of TGDDM–HHPA) are far from being saturated. In fact, at a sufficiently low concentration of sorbant, Langmuir-type isotherms approach linearity. The fact that the system at hand is far from saturation in the investigated activity range, can actually be demonstrated: the system stoichiometry indicates that the concentration of carbonyl groups is 5.3 mol kg^{-1}, while the maximum concentration of interacting water, attained at $a_w = 0.6$, is 0.38 mol kg^{-1} (see Table 1), which corresponds to only 7.2% of the available carbonyls. Analogous conclusions were drawn in the case of TGDDM–DDS [8] with reference to the relevant interacting sites (amino-alcohol and sulphonic groups).

As a consequence of the independence of ϕ on concentration, we can write:

$$\frac{\partial C_{S_0}}{\partial t} = \frac{\partial}{\partial x}\left(\phi D(C_{TOT})\frac{\partial C_{S_0}}{\partial x}\right) \tag{7}$$

Moreover, in view of the linearity of the adsorption equilibrium, it follows that:

$$C_i = C_i^0 K_i C_{S_0} \text{ and } C_{TOT} = C_{S_0}\left(1 + \sum_{i=1}^{n} K_i C_i^0\right),$$

and, consequently:

$$\frac{\partial C_i}{\partial t} = \frac{\partial}{\partial x}\left(\phi D(C_{TOT})\frac{\partial C_i}{\partial x}\right) \tag{8}$$

$$\frac{\partial C_{TOT}}{\partial t} = \frac{\partial}{\partial x}\left(\phi D(C_{TOT})\frac{\partial C_{TOT}}{\partial x}\right) = \frac{\partial}{\partial x}\left(D_{eff}(C_{TOT})\frac{\partial C_{TOT}}{\partial x}\right) \tag{9}$$

Hence, the effective mutual diffusivity coefficient, $D_{\mathrm{eff}}(C_{\mathrm{TOT}})$, which characterizes the overall sorption kinetics, can be factorized in the product of (i) a contribution consisting of a concentration dependent mutual diffusivity, $D(C_{\mathrm{TOT}})$, which takes into account free volume changes and would characterize transport through the material in the absence of the 'sticking' effect due to the molecular interactions, and (ii) an 'interaction' factor, ϕ, which accounts for the molecular interactions with specific sites:

$$D_{\mathrm{eff}}(C_{\mathrm{TOT}}) = D(C_{\mathrm{TOT}})\phi \tag{10}$$

It is worth noting that ϕ accounts for the direct effect of interactions on the diffusive movements of water molecules. Actually, establishment of water/epoxy interactions indirectly affects $D(C_{\mathrm{TOT}})$ also, since it is reasonable that these interactions do perturb the network structure as well.

From the spectroscopic data, ϕ has been calculated to be equal to 0.35 for the TGDDM–DDS resin and 0.45 for the TGDDM–HHPA, and has been found to be independent of concentration. The lower value of ϕ for the TGDDM–DDS resin, reflects the higher interaction energy of the specific sites present on the network (i.e. amino-alcohol and sulphonic groups) as compared to the case of TGDDM–HHPA (ester carbonyls).

An estimate of $D_{\mathrm{eff}}(C_{\mathrm{TOT}})$ for both resins can be obtained from the integral sorption curves (spectroscopic data from the ν_{OH} band) determined at different water vapour activities, by applying a well established procedure (see Ref. [29]). In fact, by measuring the 'half-time of sorption', $(t/L^2)_{1/2}$, (i.e. the value of t/L^2 for which $M_t/M_\infty = 1/2$ or $A_t/A_\infty = 1/2$) a value $\overline{D}_{\mathrm{eff}}$ can be determined for each sorption curve, which is some mean value of the variable diffusion coefficient averaged over the concentration range spanned in the sorption experiment. This value can be determined from the following equation [29]:

$$\overline{D}_{\mathrm{eff}} = 0.049/\left(t/L^2\right)_{1/2}$$

where L is the sample thickness. $\overline{D}_{\mathrm{eff}}$ supplies a reasonable estimate of

$$\left(1/C^0_{\mathrm{TOT}}\right)\int_0^{C^0_{\mathrm{TOT}}} D_{\mathrm{eff}}\mathrm{d}C_{\mathrm{TOT}}$$

where 0 to C^0_{TOT} is the water concentration range in the network of the sorption experiment. Once the values of $\overline{D}_{\mathrm{eff}}$ have been determined, a graph of $\overline{D}_{\mathrm{eff}}C^0_{\mathrm{TOT}}$ as a function of C^0_{TOT} can be obtained, which provides, by numerical differentiation, a first approximation to the relationship between D_{eff} and C_{TOT}.

The values of $D(C)$ can then been calculated, for each sorption test, from Eq. (10) using the corresponding values of $D_{\mathrm{eff}}(C_{\mathrm{TOT}})$, as determined by the previously outlined procedure. In Table 2 and in Fig. 13 are summarized the results obtained for both resins, which show that both D_{eff} and D are increasing functions of concentration.

The analysis of these results indicates that the TGDDM–DDS resin displays lower values for $D(C_{\mathrm{TOT}})$ and its value is also more sensitive to water concentration (see relative changes in $D(C_{\mathrm{TOT}})$). This points to a network structure which is more tightly packed than in the case of TGDDM–HHPA and, consequently, more sensitive to free volume changes associated with water sorption which perturbs the molecular structure of the polymer network. The presence of stronger interactive sites, which determine a lower value of ϕ, contributes to a further decrease of the effective diffusivity, related to the 'sticking' of water molecules on these sites. The consequences are lower values of $D_{\mathrm{eff}}(C_{\mathrm{TOT}})$ and a higher dependence on water concentration. The finding that, in the case of TGDDM–DDS, $\overline{D}_{\mathrm{eff}}$, for sorption is about 2.3 times higher than that for desorption at $a_{\mathrm{w}} = 0.4$ (see also Fig. 11) while, in the case of TGDDM–HHPA resin, this factor is around 1.4, is to be related to the discussed higher dependence of diffusivity on concentration as well as to the higher concentration range determined, at the same activity, by the higher water solubility.

The presently adopted model (Eqs. (3)–(9)) is a modified version of the approach originally developed by Carter and Kibler [30] and subsequently employed by other investigators [31]. In particular, these authors interpreted anomalous water diffusion in composite resins assuming that the diffusion of mobile molecules conforms to simple diffusion theory augmented by sources and sinks. They did not speculate on the nature of absorption sites at which water molecules became bound to the epoxy network. In their development, they further assumed that the absorption probability is remarkably small, implying that the characteristic diffusion time is much smaller than the time needed to reach final equilibrium of binding sites. In their interpretation, the spatial distribution of mobile

Table 2
Equilibrium water content, diffusivities and interaction factors for the sorption tests performed at different activities on the TGDDM–DDS and TGDDM–HHPA resins

TGDDM–DDS					TGDDM–HHPA				
C^0_{TOT} [%b.w.]	$\overline{D}_{\mathrm{eff}}$ [cm^2/s]	$D_{\mathrm{eff}}(C_{\mathrm{TOT}})$ [cm^2/s]	$D(C_{\mathrm{TOT}})$ [cm^2/s]	ϕ	C^0_{TOT} [%b.w.]	$\overline{D}_{\mathrm{eff}}$ [cm^2/s]	$D_{\mathrm{eff}}(C_{\mathrm{TOT}})$ [cm^2/s]	$D(C_{\mathrm{TOT}})$ [cm^2/s]	ϕ
0.75	2.88×10^{-10}	3.65×10^{-10}	10.4×10^{-10}	0.35	0.26	1.20×10^{-9}	2.07×10^{-9}	4.6×10^{-9}	0.45
1.61	4.30×10^{-10}	5.48×10^{-10}	15.7×10^{-10}	0.35	0.49	1.62×10^{-9}	2.13×10^{-9}	4.73×10^{-9}	0.45
2.83	4.99×10^{-10}	8.06×10^{-10}	23.0×10^{-10}	0.35	0.87	1.87×10^{-9}	2.25×10^{-9}	5.00×10^{-9}	0.45
4.07	6.48×10^{-10}	10.7×10^{-10}	30.6×10^{-10}	0.35	1.28	2.01×10^{-9}	2.37×10^{-9}	5.27×10^{-9}	0.45

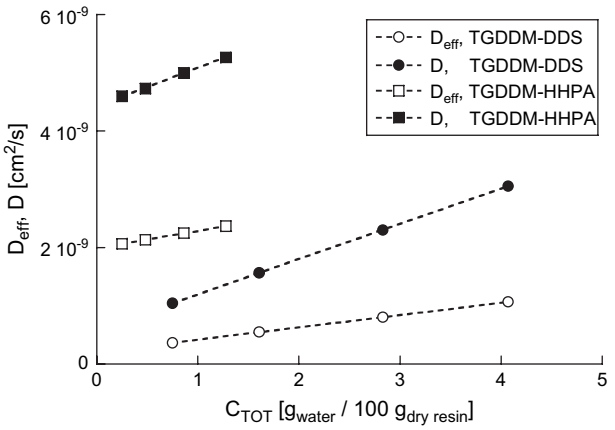

Fig. 13. Diffusivities as a function of total water concentration from sorption measurements on the TGDDM–DDS and TGDDM–HHPA resins.

molecules becomes rather uniform in the sample long before the specimen is saturated with regard to bound molecules, the ultimate saturation proceeding at the same rate everywhere in the sample. The binding capacity of the polymer matrix is actually promoted by long term relaxation phenomena which expose originally inaccessible binding sites. In the work of the above authors, the experimental time was of the order of several years, while, in the present analysis, it is of the order of tenths of minutes, i.e. much shorter than the time needed for the aging processes to take place. The same arguments justify the absence of long term hygrothermal degradation, reported by other investigators [32,33]. The stability of our samples in the present experimental conditions is unambiguously demonstrated by the coincidence of the spectra of the specimens prior and after a sorption–desorption cycle (see trace F in Fig. 5). On the basis of the spectroscopic evidence, we have made the hypothesis that the characteristic time of the binding process is much smaller than the characteristic time of diffusion, leading us to assume an 'instantaneous' (in relative terms) establishment of the local binding equilibrium. The contradiction between this hypothesis and that adopted by Carter and Kibler is only apparent and is due to the different meaning attributed by these authors to the term 'bound water'.

4. Conclusions

Time-resolved FTIR and gravimetric analysis were employed to investigate the mass transport of water in a TGDDM–HHPA epoxy network. The spectroscopic analysis evidenced the presence of non-interacting water molecules together with distinct H-bonded water species. The evaluation of the molar absorptivities of the different species allowed us to estimate equilibrium concentrations that are in excellent agreement with the results of gravimetric measurements.

The occurrence of an instantaneous linear equilibrium among the different water species was inferred from the kinetic behaviour of the different components and from the dependence of the equilibrium values on concentration.

The transport of water was found to follow a Fickian behaviour characterized by an effective mutual diffusion coefficient, $D_{\mathrm{eff}}(C_{\mathrm{TOT}})$, which increases with total water concentration. The dependence of D_{eff} on concentration, as obtained from integral sorption curves, has been interpreted by introducing a concentration dependent term, $D(C_{\mathrm{TOT}})$, and an 'interaction factor', ϕ, accounting for the effect of H-bonding with specific sites on the polymer network, which effectively slow down the diffusion process. The analysis has been based on a simple model, already adopted in a previous contribution, which assumes immobilization of water molecules H-bonded to specific sites on the polymer backbone and instantaneous attainment of a local linear equilibrium among the different species.

Comparison of these results with a similar analysis of water transport on another epoxy network, TGDDM–DDS, characterized by the presence of stronger interacting sites, evidenced differences and similarities which can be justified on the basis of the differences in the network structure, i.e. type of interacting sites and network molecular structure.

References

[1] May CA, editor. Epoxy resins, chemistry and technology. 2nd ed. New York: Marcel Dekker Inc.; 1988.
[2] Lee H, Neville K. Handbook of epoxy resins. New York: McGraw-Hill; 1990.
[3] Ellis B, editor. Chemistry and technology of epoxy resins. Glasgow: Blackie Academic and Professional; 1993.
[4] Lin SC. High performance thermosets: chemistry, properties and applications. Munich: Hanser; 1994.
[5] Majerus MS, Soong DS, Prausnitz JM. J Appl Polym Sci 1984;29:2453.
[6] McKague EL, Reynolds JD, Halkies JE. J Appl Polym Sci 1978;22:1643.
[7] Mijovic J, Lin K. J Appl Polym Sci 1985;30:2527.
[8] Cotugno S, Mensitieri G, Musto P, Sanguigno L. Macromolecules 2005;38:801.
[9] Fieldson GT, Barbari AT. Polymer 1993;34(6):1146.
[10] Van Alsten JG. Trends Polym Sci 1995;3(8):272.
[11] Hong SU, Barbari AT, Sloan JM. J Polym Sci Part B Polym Phys 1998;36:337.
[12] Cotugno S, Larobina D, Mensitieri G, Musto P, Ragosta G. Polymer 2000;42:6431.
[13] Musto P, Mascia L, Ragosta G, Scarinzi G, Villano P. Polymer 2000;41:565.
[14] Wu P, Siesler HW. Macromol Symp 1999;143:323.
[15] Mensitieri G, Cotugno S, Musto P, Ragosta G, Nicolais L. Transport of water in high T_g polymers: a comparison between interacting and non-interacting systems. In: Mittal KL, editor. Polyimides and other high temperature polymers: synthesis, characterization and applications, vol. 2. The Netherlands: VSP Publ.; 2003.
[16] Koenig JL. Spectroscopy of polymers. Washington, DC: American Chemical Society; 1992.
[17] Krishnan K, Ferraro JR. In: Ferraro JR, Basile LJ, editors. Fourier transform infrared spectroscopy, vol. 3. New York: Academic Press; 1982. p. 198.
[18] Marquardt DW. J Soc Ind Appl Math 1963;11:441.
[19] Maddams WF. Appl Spectrosc 1980;34:245.
[20] Meier RJ. Vib Spectrosc 2005;39:266.
[21] Pimentel GC, McClellan AL. The hydrogen bond. San Francisco, USA: W.H. Freeman and Co. Publ.; 1960.
[22] Murthy ASN, Rao CNR. Appl Spectrosc Rev 1968;2(1):69.

[23] George WO, Lewis R. Hydrogen bonding. In: Chalmers JM, Griffiths PR, editors. Handbook of vibrational spectroscopy, vol. 3. Chichester, UK: Wiley; 2002. p. 1919.
[24] Fredericks SY, Jordan K, Zwier TS. J Phys Chem 1996;100:7810.
[25] Antoon MK, Koenig JL, Serafini T. J Polym Sci Polym Phys Ed 1981; 19:1567.
[26] Ngono Y, Maréchal Y, Mermilliod N. J Phys Chem B 1999;103:49.
[27] Huggins CM, Pimentel GC. J Phys Chem 1956;60:1615.
[28] Mirone P, Fabbri GF. Gazz Chim Ital 1956;86:1079.
[29] Crank J. The mathematics of diffusion. 2nd ed. Oxford: Clarendon Press; 1975.
[30] Carter HG, Kibler KG. J Compos Mater 1978;12:118.
[31] Popineau S, Rondeau-Mouro C, Sulpice-Gaillet C, Shanahan MER. Polymer 2005;46:10733.
[32] Xiao GZ, Shanahan MER. J Appl Polym Sci 1998;69:363.
[33] Xiao GZ, Shanahan MER. J Polym Sci Part B Polym Phys 1997;35:2659.